**Proceedings of the ASME 2010 International Design Engineering Technical Conferences & Computers and Information in Engineering Conference**
**IDETC/CIE 2010**
**August 15-18, 2010, Montreal, Quebec, Canada**

**DETC2010-28022**

# AN INTELLIGENT EXOSKELETON FOR LOWER LIMB REHABILITATION

**Hashem Ashrafiuon*, Kent Grosh, Kevin J. Burke, and Kathleen Bommer**
Center for Nonlinear Dynamics and Control,
Villanova University, Villanova, PA, 19085
* Corresponding Author, Email: hashem.ashrafiuon@villanova.edu

## ABSTRACT

A lightweight adjustable exoskeleton is designed to exercise human legs of varying size and weights. The exoskeleton is actuated by three DC motors at the hip, knee, and ankle. An experimental setup with motor controllers, power supplies, a controlled board, and a computer is developed for closed loop control. A sliding mode control law is designed and implemented to exercise an articulated mannequin leg. It is shown that the exoskeleton is able to adapt to external forces making it suitable to aid in the human leg rehabilitation process.

## 1 INTRODUCTION

Rehabilitation is a required but difficult process for patients trying to recover the full control of their hips, knees, or other parts of their body. Some of the most important types of rehabilitation include neuromuscular rehabilitation for neutrally impaired patients due to spinal cord injury and muscle/ligament rehabilitation for patients with hip, knee, or ankle replacement surgery. Spinal cord is capable of relearning the ability to walk through proper training even when cut off from the brain [1, 2]. A large proportion of people with spinal cord injury who sustain motor incomplete lesions can regain some recovery in their walking ability. Symmetrical movements of lower extremities consistent with normal physiological gait patterns provide critical sensory cues necessary for maintaining and enhancing walking ability [3].

While procedures such as hip replacement surgery can be very beneficial, the best way to maximize those benefits is through proper rehabilitation. The American Academy of Physical Medicine and Rehabilitation says as Baby Boomers age, the number of total hip replacements is expected to increase by more than 60 percent in the next 30 years. Physical therapy is extremely important in the overall outcome of any joint replacement surgery. The goals of physical therapy are to prevent contractures, improve patient education, and strengthen muscles through controlled exercises. Contractures result from scarring of the tissues around the joint. Contractures do not permit full range of motion, and therefore impede mobility of the replaced joint.

A promising solution for rehabilitation of patients with spinal cord injury, those with joint replacement surgery, and many other mobility-impaired patients, is to design exoskeletal devices. It has already been shown that motorized robotic-assisted devices can be very helpful in training individuals to regain their walking ability following motor incomplete spinal cord injury [4]. Exoskeletal devices have the potential to be used during sitting, standing, and walking stages of rehabilitation. The study of the exoskeletal power assist systems was first initiated in the late 1960's on a 30-DOF full-body exoskeleton which was called Hardiman [5]. Another early suggested exoskeleton was a 7-DOF man-amplifying arm with two-axis (universal) joints [6]. Exoskeletal systems have also been suggested as rehabilitative tools. A driven gait orthosis has been developed that can move patient's legs on a treadmill [7]. Another device has been developed to provide walking aid for people with gait disorder [8]. This device has a hybrid control system that consists of posture and power-assist control based on biological feedback. The actuators are DC servomotors generating assist moments at the hip and the knee joints.

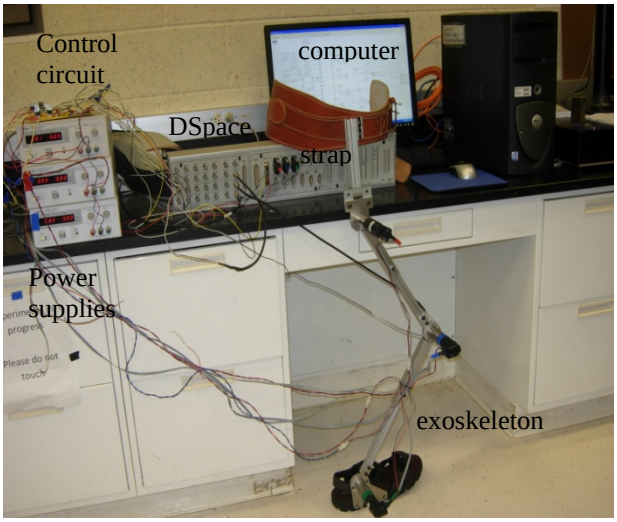


Figure 1. The exoskeleton and its experimental setup

Other exoskeletal devices include BLEEX which was developed in 2004 at the Human Engineering Laboratory of University of California, Berkeley [9]. The operational concept of BLEEX is that the human provides an intelligent control system for the exoskeleton while the exoskeleton actuators provide the necessary strength for walking. A pneumatically actuated exoskeleton [10] and a powered lower limb orthoses [11] have been developed for nurses and gait rehabilitation, respectively. Researchers have suggested an exoskeletal power assistance device for the knee using series elastic actuators [12] and a lightweight exoskeleton that uses adjustable graphite/epoxy struts and is attached to the body by belts [13]. A gravity-balancing device has been developed for single human leg during motion [14]. A motorized crutch device [15] and a tendon-driven exoskeletal power assistance device [16] have also been suggested to enhance the mobility of individuals with lower limb disabilities. There are also many single or double joint active orthoses for knee and knee and ankle [17]. A comprehensive review of lower extremity exoskeletons is presented in [18].

The purpose of this work is to design a lightweight, exoskeletal device that can easily be adjusted and worn by people of different sizes for leg exercises and rehabilitation after hip, knee, or ankle replacement surgeries. In the following sections, the exoskeleton design, its experimental setup, and mathematical model are presented. Next, a model-based robust control design that can adapt to patient's ability is described. Finally, simulation and experimental results with a mannequin leg are presented to verify the performance of the device.

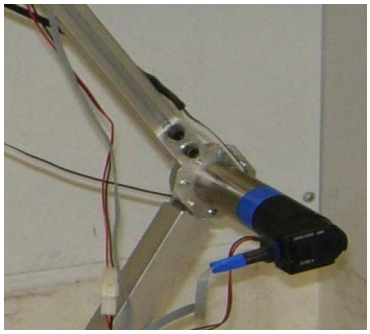

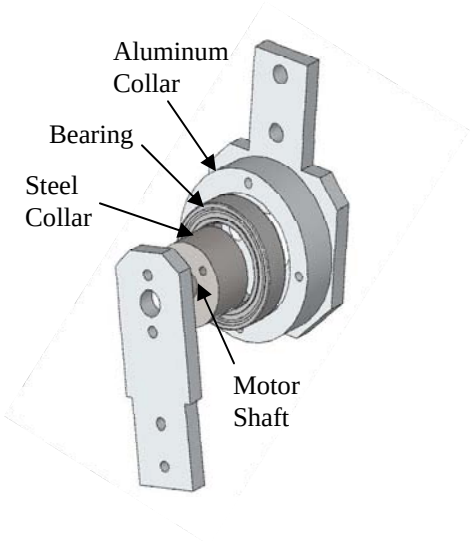


Figure 2. The exoskeleton joint design and motor

## 2 THE EXOSKELETON DESIGN

A picture of the exoskeleton and its experimental setup is shown in Fig. 1. The exoskeleton is designed with four links: upper body, femur, tibia, and foot. The upper body is equipped with a link and a large strap such that it can be attached around the waist. Currently, the upper body is strapped around a fixed object such that the exoskeleton can be used to exercise the leg while standing (or sitting).

The links are connected through revolute joints which are operated by three 7 Nm low voltage DC motors. A simple structural Aluminum framing system with T-slots was used to construct the links, allowing for easily adjustable link lengths. A simple bearing within two collars was designed and fabricated, distributing the load parallel to the primary axis of the leg and away from the shaft of the motor. This system provided easy addition or removal of the motors and weighs approximately 1.5 kg without the motors. Each motors weighs about .69 kg. A diagram of the joint design and a picture of the knee joint and its DC motor are shown in Fig. 2.

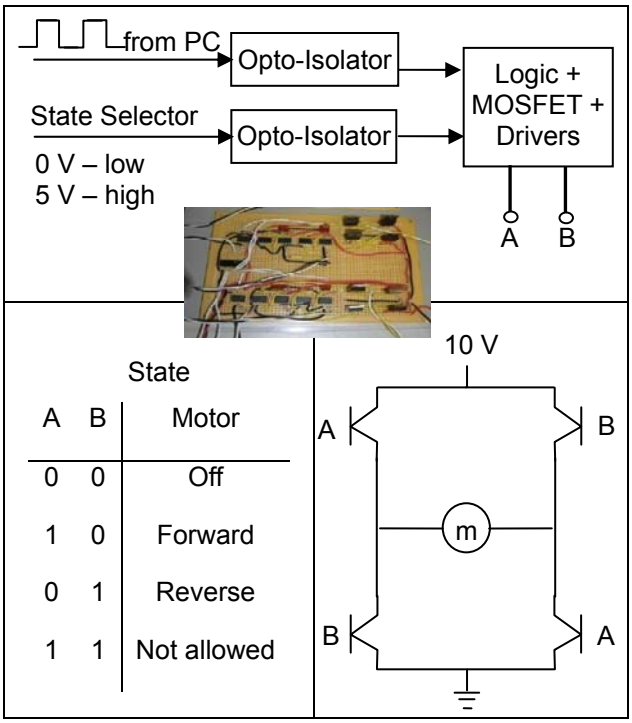


Figure 3. The control circuit H-Bridge design

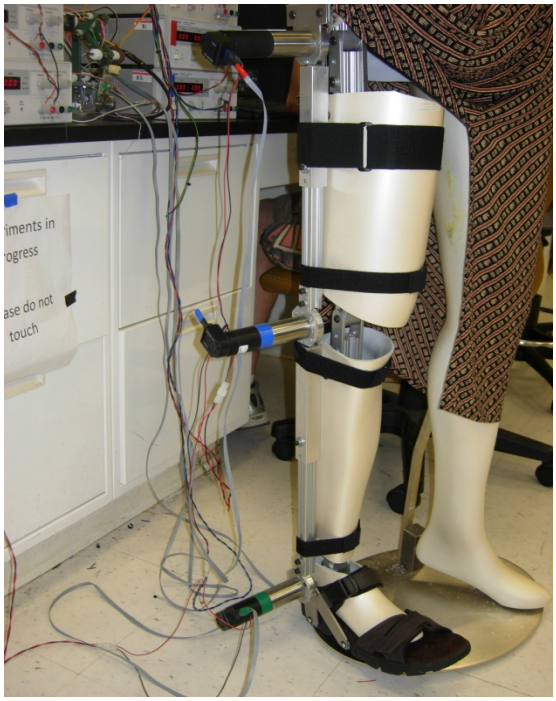

Figure 4. The exoskeleton with an articulated mannequin right leg

The experimental setup includes a computer where the control law is implemented based the joint angle feedback received from the DC motor encoders. A DSpace™ board is then used to output the control signals. The control signals are then processes and amplified through a control circuit and power supplies and passed to the DC motors.

Three power supplies are necessary to control the exoskeleton. A PWM (pulse-width modulation) system is used, in which the DSpace™ outputs a square wave pulse signal at 10 V and 20 kHz where the length of the pulses determine motor speed and torque. The remaining two power supplies serve as amplifiers. Hence, no additional power supplies would be if more motors are added.

The power supplies supply a 0-20V output at up to 3A. However, the motors require positive and negative signals for forward and backward motion, respectively. A circuit was designed, as shown in Fig. 3, to rapidly change the sign of the signals based on the typical H-Bridge design. The circuit receives a square wave with a specific duty cycle to control the speed plus a control line for its direction. Depending on the state of the control line, low or high, the circuit sends the square wave with proper current to drive the A or B transistor set in the bridge. The logic in the controller prevents A and B from activating at the same time and creating a faulty condition, and optically isolates the H bridge from the control computer.

A typical clothing store mannequin was revised to add articulation to test with the exoskeleton. The mannequin right leg was segmented and metal parts were inserted with very low friction revolute joints at hip, knee, and ankle. The mannequin is shown assembled on the exoskeleton in Fig. 4. The upper body part of the exoskeleton is strapped around the mannequin waist (not shown).

## 3 THE EXOSKELETON MODEL

The planar 3DOF model of the exoskeleton is shown in Fig. 5 where $l_i$, $m_i$, $I_i$, and $d_i$, represent length, mass, mass moment of inertia, and distance from joint to the center of mass of link *i*. The three moving links are the femur, the tibia, and the foot while the upper body is fixed to ground. The joint angles $\theta_1, \theta_2, \text{and } \theta_3$ are measured counterclockwise and represent the hip, knee, and ankle, respectively.

The equations of motion of the system in terms of the three joint angles can be written in vector form as:

$$M(\boldsymbol{\theta})\ddot{\boldsymbol{\theta}} + \boldsymbol{f}(\boldsymbol{\theta}, \dot{\boldsymbol{\theta}}) + \boldsymbol{g}(\boldsymbol{\theta}) = \boldsymbol{\tau} + \boldsymbol{\tau}'$$

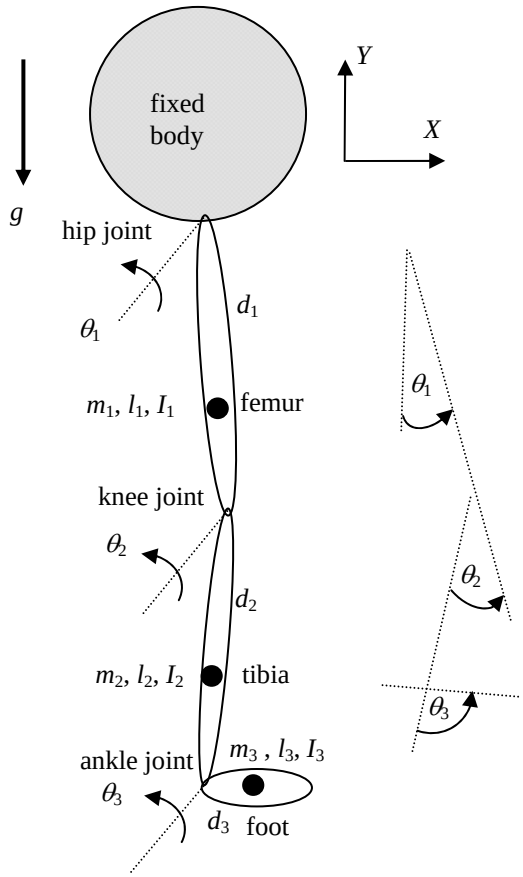


Figure 5. The exoskeleton model

where $M \in \mathbb{R}^{3\times3}$ is the positive definite mass matrix, $\boldsymbol{f} \in \mathbb{R}^3$ is the vector of centrifugal and coriolis moments, $\boldsymbol{g} \in \mathbb{R}^3$ is the vector of gravitational moments, $\boldsymbol{\tau} \in \mathbb{R}^3$ is the vector of motor torque, $\boldsymbol{\tau'} \in \mathbb{R}^3$ is the vector of frictional moments, and $\boldsymbol{\theta}$, $\dot{\boldsymbol{\theta}}$, $\ddot{\boldsymbol{\theta}} \in \mathbb{R}^3$ are the joint position, velocity and acceleration vectors, respectively.

The elements of $M$, $\boldsymbol{g}$, and $\boldsymbol{f}$ may respectively be written as:

$$M_{11} = a_5 + 2(a_4C_2 + a_2C_{23} + a_1C_3)$$
$$M_{12} = a_3 + a_4C_2 + a_2C_{23} + 2a_1C_3$$
$$M_{22} = I_2 + a_3 + 2a_1C_3$$
$$M_{13} = a_1C_3 + a_2C_{23}$$
$$M_{23} = a_1C_3$$
$$M_{33} = I_3 + m_3d_3^2$$

$$g_3 = b_3S_{123}$$
$$g_2 = g_3 + b_2S_{12}$$
$$g_1 = g_2 + b_1S_1$$

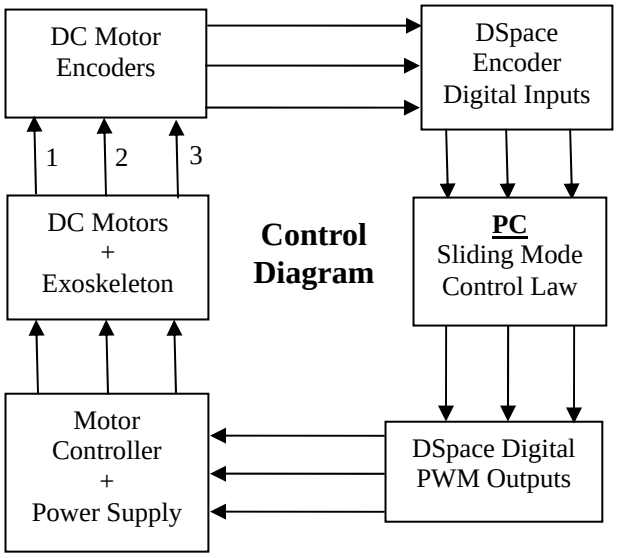


Figure 6. The control system block diagram

$$f_1 = -a_4S_2(2\dot{\theta}_1 + \dot{\theta}_2)\dot{\theta}_2 - [a_1S_3\dot{\theta}_3 + a_2S_{23}(\dot{\theta}_2 + \dot{\theta}_3)](2\dot{\theta}_1 + 2\dot{\theta}_2 + \dot{\theta}_3)$$

$$f_2 = (a_4S_2 + a_2S_{23})\dot{\theta}_1^2 - a_1S_3(2\dot{\theta}_1 + 2\dot{\theta}_2 + \dot{\theta}_3)\dot{\theta}_3$$

$$f_3 = a_2S_{23}\dot{\theta}_1^2 + a_1S_3(\dot{\theta}_1^2 + \dot{\theta}_2^2 + \dot{\theta}_1\dot{\theta}_2)$$

where the notation $C_i \equiv \cos\theta_i$, $C_{ij} \equiv \cos(\theta_i + \theta_j)$, $C_{ijk} \equiv \cos(\theta_i + \theta_j + \theta_k)$, $S_i \equiv \sin\theta_i$, $S_{ij} \equiv \sin(\theta_i + \theta_j)$, $S_{ijk} \equiv \sin(\theta_i + \theta_j + \theta_k)$ is used and the following constants are defined in terms of the systems physical parameters:

$$a_1 = m_3l_2d_3$$
$$a_2 = m_3l_1d_3$$
$$a_3 = m_2d_2^2 + m_3(l_2^2 + d_3^2)$$
$$a_4 = (m_2d_2 + m_3l_2)l_1$$
$$a_5 = I_1 + m_1d_1^2 + (m_2 + m_3)l_1^2 + a_3$$

$$b_1 = m_1gd_1 + m_2gl_2 + m_3gl_3$$
$$b_2 = m_2gd_2 + m_3gl_3$$
$$b_3 = m_3gd_3$$

In the above equations, g is acceleration due to gravity. The frictional moments are simply defined as a combination of viscous and dry friction as:

$$\tau'_i = -B_i\dot{\theta}_i - B'_i sgn(\dot{\theta}_i), \qquad i = 1,2,3$$

## 4 CONTROL DESIGN

A sliding mode control law [18,19] is derived for the exoskeleton following the procedure described in [20]. In this method, a first order exponentially stable surface, $s_i$, is defined in terms of each joint angle tracking errors. Then, a control law is determined that guarantees all system trajectories reach these surfaces in finite time (reaching phase) and hence exponentially slide to the origin (sliding phase). The three first-order surfaces, $\boldsymbol{s} \in \mathbb{R}^3$, are defined as:

$$\boldsymbol{s} = \left(\dot{\boldsymbol{\theta}} - \dot{\boldsymbol{\theta}}^{\mathrm{d}}\right) + \Lambda\left(\boldsymbol{\theta} - \boldsymbol{\theta}^{\boldsymbol{d}}\right)$$

where the superscript "*d*" denotes the desired trajectory and $\Lambda \in \mathbb{R}^{3\times3}$ is a positive definite diagonal matrix with parameters $\lambda_i$, $i = 1,2,3$. Taking the time derivative of the surfaces results in

$$\dot{\boldsymbol{s}} = \ddot{\boldsymbol{\theta}} - \dot{\boldsymbol{s}}_r \ , \quad \dot{\boldsymbol{s}}_r = \ddot{\boldsymbol{\theta}} - \Lambda\left(\dot{\boldsymbol{\theta}} - \dot{\boldsymbol{\theta}}^{\mathrm{d}}\right)$$

The control law is obtained by substituting $\ddot{\boldsymbol{\theta}}$ from Eq. (x) and subtracting a robustness term $\boldsymbol{k} \circ sgn(\boldsymbol{s})$ as discussed in [21]

$$\boldsymbol{\tau} = \boldsymbol{f} + \boldsymbol{g} - \widehat{\boldsymbol{\tau}'} + \boldsymbol{M}\dot{\boldsymbol{s}}_r - \boldsymbol{k} \circ sgn(\boldsymbol{s})$$

where "∘" is used for element-wise multiplication and $\widehat{\boldsymbol{\tau}'}$ represents the nominal value of $\boldsymbol{\tau}'$. Here we are assuming that the only uncertainty in the model comes from the frictional moments since very accurate mass and geometric properties are available. Hence, vector $\boldsymbol{k}$ may be defined as:

$$\boldsymbol{k} = \boldsymbol{T}' + \boldsymbol{\eta}$$

where $\boldsymbol{\eta} \in \mathbb{R}^3$ contains the positive effort parameters that determine how fast the reaching phase of the trajectory is completed. Elements of $\boldsymbol{T}' \in \mathbb{R}^3$ define the bounds on the uncertainty in the frictional moments:

$$|\tau_i - \tau'_i| \le T'_i \ , \qquad i = 1,2,3$$

Hence, if we define $V = \frac{1}{2}\boldsymbol{s}^T\boldsymbol{s}$ as a Lyapunov candidate function, it can be easily shown that

$$\dot{V} = \boldsymbol{s}^T\dot{\boldsymbol{s}} \le -\boldsymbol{\eta}^T\boldsymbol{M}^{-1}|\boldsymbol{s}|$$

Thus, the trajectory reaches the surfaces in finite time and then slides to the origin.

## 5 RESULTS

The control system is initially simulated followed by experimental implementation. It is implemented by reading the encoder signals which provide joint angles $\boldsymbol{\theta}$ and velocities $\dot{\boldsymbol{\theta}}$ feedback. The control signals are sent in PWM form to the motor controller and power supplies which drive the DC motors. The block diagram of the closed-loop control system setup is shown in Fig. 6.

Since the sliding mode control results in chattering due to the use of the robustness term $\boldsymbol{k} \circ sgn(\boldsymbol{s})$, we have approximated this discontinuous function with a continuous saturation function $\boldsymbol{k} \circ sat(\boldsymbol{s}/\boldsymbol{\phi})$ where $\boldsymbol{\phi} \in \mathbb{R}^3$ represents the boundary layer thicknesses for the three surfaces. However, this only guarantees trajectory convergence to the region around the surfaces with the corresponding boundary layers [21]. Hence, larger $\boldsymbol{\phi}$ results in more error and less chattering and thus a compromise must be made when selecting these parameters.

The exoskeleton's physical properties are listed in Table 1. The values within parentheses are the ones with the mannequin which are the ones used for the experiment. The $V_{min}$ values are the experimentally derived minimum voltages required to move each joint. The control law tuning parameters, $\lambda_i$, $\eta_i$, and $\phi_i$, are listed in Table 2. These parameters are selected based on the desired performance/ robustness tradeoff of the controller and the limitations of the actuators.

Table 1. Physical properties of the exoskeleton. " ()" indicate values for exoskeleton and the mannequin.

| Link no. | 1 | 2 | 3 |
|---|---|---|---|
| $l_i$ (m) | .37 | .44 | .22 |
| $d_i$ (m) | .30 (.24) | .36 (.28) | .11 (.11) |
| $m_i$ (kg) | 1.09 (2.39) | 1.09 (2.39) | .40 (.80) |
| $I_i$ (kg.m$^2$) | .013 (.036) | .019 (.051) | .002 (.005) |
| $B_i$ (N.m.s/rad) | 27 | 22 | 15 |
| $B'_i$ (N.m) | 2.4 | 2.4 | 2.4 |
| $V_{min}$ (V) | .4 | 1.4 | .96 |

Table 2. Sliding mode control tuning parameters

| Surface no. | 1 | 2 | 3 |
|---|---|---|---|
| $\lambda_i$ | 2 | 2 | 2 |
| $\eta_i$ | 15 | 25 | 25 |
| $\phi_i$ | .15 | .15 | .15 |

As an example, it is desired to rotate the joint angles from $[0° \ 0° \ 90°]$ to $[30° \ -60° \ 70°]$ starting from rest and ending at rest in 15 seconds. The exoskeleton is then commanded to rotate back

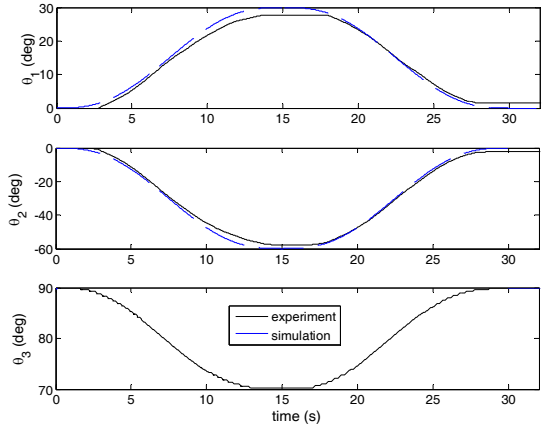


Figure 7. Comparison of joint angle trajectories derived from simulation and experiment

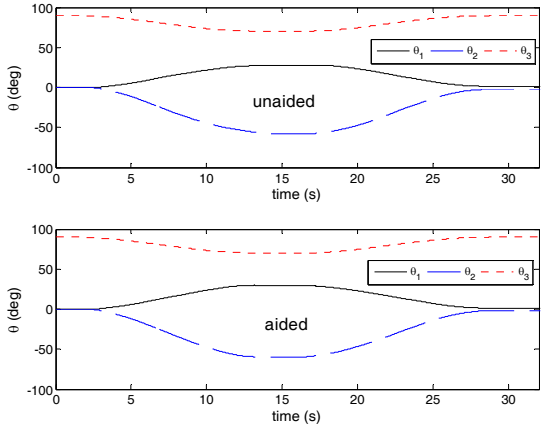


Figure 8. Experimental joint angle plots for unaided and aided cases

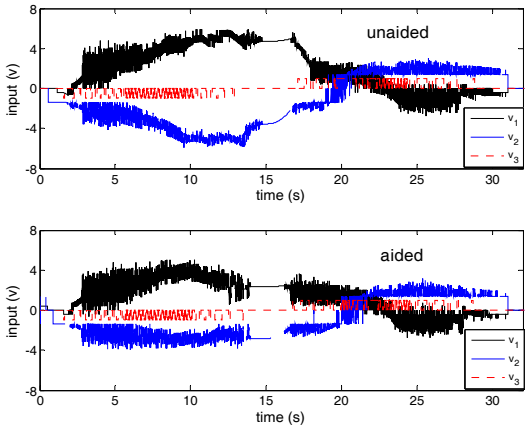


Figure 9. Experimental control voltage plots for unaided and aided cases

to the original configuration in exactly the same manner. Hence, the desired trajectories, $\boldsymbol{\theta^d}$, are generated as fifth-degree polynomials using zero initial and final joint velocities and accelerations.

Figure 7 shows the performance of the controller in moving the joints according the desired fifth-order polynomial trajectories for both simulation and experiment. The simulation results perfectly follow the desired trajectories. The trajectories obtained from experiment closely follow those of the simulations but do have some visible error. The error is mainly due to our estimate of motor stiction.

Next, the previous experiment was repeated once without any outside interference (unaided) and once with human interference (aided). In the latter case, we pushed both the femur and tibia in the direction of the motion in order to simulate a patient trying to exercise their hip and knee. Figure 8 shows the controller is able to follow the desired trajectories in the "aided" case just as well as the "unaided" case and hence is able to adapt to the patient's ability. Figure 9 shows the control voltages for the "unaided" and "aided" cases. The figure clearly demonstrates that the smaller voltages are applied to the hip and knee motors when the femur and tibia are being aided in their motion. Note that, the control voltage applied to the ankle is less than the minimum required for motion. This is why the applied voltage looks like a series of impulses.

## 6 CONCLUSIONS

An intelligent exoskeleton is designed and presented which can be used for rehabilitation of hip, knee, and/or ankle joints. A model based robust sliding mode control law is implemented to perform the prescribed rehabilitative exercises. The exoskeleton is shown to effectively perform when commanded to exercise a mannequin leg. It is further shown to be adaptive to external forces making it suitable for use with actual patients. In future, a second leg will be designed to complete a full exoskeleton that can be worn to enable paraplegic patients to walk.

## ACKNOWLEDGEMENTS

This research was partially supported by the 2009 Delaware County, Pennsylvania, Keystone Innovation Grant. Support for this work from the Center for Nonlinear Dynamics and Control (CENDAC) at Villanova University is also acknowledged.

## REFERENCES


[1] I. Wickelgren, I., "Teaching the spinal cord to walk," *Science*, **279**, 1998, pp.319–321.

[2] Behrman, A. L., and Harkema, S. J., "Locomotor training after human spinal cord injury: a series of case studies," *Physical Therapy*, **80** (7), 2000, pp. 688–700.

[3] Wang, C.-Y. E., Bobrow, J. E., and Reinkensmeyer, D. J., "Dynamic motion planning for the design of robotic gait rehabilitation," *Journal of Biomechanical Engineering*, **127**, 2005, pp.672–679.

[4] Hornby, T. G., Zemon, D. H., and Campbell, D., "Robotic-assisted, body-weight-supported tread-mill training in individuals following motor incomplete spinal cord injury," *Physical Therapy*, **85** (1), 2005, pp.52–66.

[5] Mosher, R. S., "Handyman to hardiman," *SAE Automotive Engineering Congress*, Detroit, MI, SAE paper no. 670088, 1967.

[6] Rosheim, M. E., "Man-amplifying exoskeleton," *SPIE, Mobile Robots IV*, **1195**, 1989, pp. 402–411.

[7] Colombo, G., Jrg, M., and Dietz, V., "Driven gait orthosis to do locomotor training of paraplegic patients," *Proceedings of the 22nd Annual EMBS International Conference*, Chicago, IL, July 23-28, 2000, pp. 3159–3163.

[8] Kawamoto, H., Lee, S., Kanbe, S., and Sankai, Y., "Power assist method for HAL-3 using emg-based feedback controller," *International Conference on Control, Automation and Systems*, 2003, pp. 1648–1653.

[9] Kazerooni, H., and Steger, R., "The Berkeley lower extremity exoskeleton," *Journal of Dynamic Systems Measurement and control*, **128** (1), 2006, pp. 14-25.

[10] Yamamoto, K., Ishii, M., Noborisaka, H., and Hyodo, K., "Stand alone wearable power assisting suit -sensing and control systems, *Proceedings of IEEE International Workshop on Robot and Human Interactive Communication*, 2004, pp. 661–666.

[11] D. P. Ferris, G. S. Sawicki, and A. R. Domingo. Powered lower limb orthoses for gait rehabilitation. *Topics in Spinal Cord Injury Rehabilitation*, 11(2):34–49, 2005.

[12] Pratt, J. E., Krupp, B. T., Morse, J. C., and Collins, S. H., "The roboknee: An exoskeleton for enhancing strength and endurance during walking. *Proceedings of IEEE International Conference on Robotics and Automation*, 2004, pp. 2430–2435.

[13] Agrawal, S. K., and Fattah, A., "Theory and design of an orthotic device for full or partial gravity-balancing of a human leg during motion," *IEEE Transactions on Neural Systems and Rehabilitation Engineering*, **12** (2), 2004, pp. 157–165.

[14] Acosta-Marquez, C., and Bradley, D. A., "The analysis, design and implementation of a model of an exoskeleton to support mobility," *Proceedings of the IEEE 9th International Conference on Rehabilitation Robotics*, Chicago, IL, June 28 -July 1, 2005, pp. 99–102.

[15] Kong, K., and Jeon, D., "Design and control of a new tendon-driven exoskeletal lower body power assistive device. *Proceedings of ASME IMECE, paper no 80800*, 2005, pp. 661–666.

[16] Mavroidis, C., et al., "Smart portable rehabilitation devices," *Journal of Neuroengi-neering and Rehabilitation*, **18** (2), 2005.

[17] Dollar, A. M., and Herr, H., "Lower extremity exoskeletons and active orthoses: challenges and state-of-the-art," *IEEE Transactions of Robotics*, **24** (1), 2008, pp. 144-158.

[18] Utkin, V. I., "Variable structure systems with sliding modes," *IEEE Transactions on Automatic Control*, **22** (2), 1977, pp. 212-222.

[19] Hung, J. Y., Gao, W., Hun, J. C., "Variable structure control: a survey," *IEEE Transactions on Industrial Electronics*, **40** (1), 1993, pp. 2-22.

[20] Slotine, J.-J. E., and Li, W., "Applied Nonlinear Control," Prentice Hall, Englewood Cliffs, NJ, 1991.

[21] Khalil, H. K., "Nonlinear Systems". Prentice-Hall, Upper Saddle River, NJ, 1996.